Molecular Pharmacology Fast Forward. Published on June 4, 2014 as DOI: 10.1124/mol.114.092338
Molecular Pharmacology Fast Forward. Published on June 4, 2014 as doi:10.1124/mol.114.092338
This article has not been copyedited and formatted. The final version may differ from this version.

Gating pore currents demonstrate selective and specific modulation of individual sodium channel voltage sensors by biological toxins.

Yucheng Xiao, Kenneth Blumenthal and Theodore R. Cummins

Department of Pharmacology and Toxicology, Indiana University School of Medicine, Indianapolis, Indiana 46202 (Y.X., T.R.C.),

Department of Biochemistry, School of Medicine and Biomedical Sciences, State University of New York, Buffalo, New York 14214, USA (K.B.)

Downloaded from molpharm.aspetjournals.org at ASPET Journals on April 20, 2024

Copyright 2014 by the American Society for Pharmacology and Experimental Therapeutics.

Molecular Pharmacology Fast Forward. Published on June 4, 2014 as DOI: 10.1124/mol.114.092338
This article has not been copyedited and formatted. The final version may differ from this version.

Running title: Selective voltage sensor modulation by biological toxins

Corresponding author: Dr. Theodore R. Cummins, Department of Pharmacology and Toxicology, Stark Neurosciences Research Institute, Indiana University School of Medicine, Indianapolis, Indiana 46202, USA. Email: trcummin@iu.edu.

Number of Text Pages: 23

Number of Tables: 0

Number of Figures: 8

Number of References: 37

Number of Words in Abstract: 245

Number of Words in Introduction: 451

Number of Words in Discussion: 1125

Abbreviations:

anthopleurin B, ApB; domains I-IV, DI-DIV; HEK293, human embryonic kidney 293; HWTX-IV, huwentoxin-IV; Na_v, voltage-gated sodium channel; transmembrane segments 1-6, S1-S6; TTX, tetrodotoxin; WT, wild type; Voltage-gated sodium channels, VGSCs; wild-type, WT;

Downloaded from molpharm.aspetjournals.org at ASPET Journals on April 20, 2024

Molecular Pharmacology Fast Forward. Published on June 4, 2014 as DOI: 10.1124/mol.114.092338
This article has not been copyedited and formatted. The final version may differ from this version.

Abstract

Voltage gated sodium channels are critical determinants of nerve and muscle excitability. While numerous toxins and small molecules target sodium channels, identifying the mechanisms of action is challenging. Here we used gating pore currents selectively generated in each of the voltage-sensors from the four alpha-subunit domains (DI-DIV) to monitor the activity of individual voltage-sensors and to investigate the molecular determinants of sodium channel pharmacology. The tarantula toxin HWTX-IV, which inhibits sodium channel current, exclusively enhanced inward gating pore currents through the DII voltage-sensor. By contrast, the tarantula toxin ProTx-II, which also inhibits sodium channel currents, altered the gating pore currents in multiple voltage-sensors in a complex manner. Thus while HWTX-IV inhibits central pore currents by selectively trapping the DII voltage-sensor in the resting configuration, ProTx-II seems to inhibit central pore currents by differentially altering the configuration of multiple voltage-sensors. The sea anemone toxin anthopleurin B, which impairs open-channel inactivation, exclusively enhanced inward gating pore currents through the DIV voltage-sensor. This indicates that trapping the DIV voltage-sensor in the resting configuration selectively impairs open-channel inactivation. Furthermore, these data indicate that while activation of all four voltage-sensors is not required for central pore current generation, activation of the DII voltage-sensor is crucial. Overall, our data demonstrate that gating pore currents can determine the mechanism of action for sodium channel gating modifiers with high precision. We propose this approach could be adapted to identify the molecular mechanisms of action for gating modifiers of various voltage gated ion channels.

Downloaded from molpharm.aspetjournals.org at ASPET Journals on April 20, 2024

Molecular Pharmacology Fast Forward. Published on June 4, 2014 as DOI: 10.1124/mol.114.092338
This article has not been copyedited and formatted. The final version may differ from this version.

Introduction

Voltage-gated sodium channels (VGSCs) are the primary generator of the upstroke of the action potential in electrically excitable cells and abnormalities in VGSCs contribute to numerous inherited and acquired disorders of excitability (George, 2005; Waxman et al., 2000). A multitude of animals toxins target sodium channel voltage-sensors (Blumenthal and Seibert, 2003; Catterall, 2002; Cestele and Catterall, 2000). Many of these agents alter sodium current activity and channel gating with distinct voltage-dependent properties, suggesting that they differentially impact the voltage-sensors of VGSCs. However it can be difficult to determine the precise mechanism of action of agents that target the gating activity of sodium channels.

VGSCs are complex transmembrane proteins composed of 24 transmembrane segments (Figure 1A) arranged in 4 homologous domains (DI-DIV), each having 6 transmembrane segments (S1-S6). The central pore of the channel is formed by the S5-S6 regions of each domain and the voltage-sensors by the S1-S4 regions. The highly charged S4-segments (Figure 1B) in these complexes are surrounded by aqueous crevices that extend into the membrane from both the extracellular and intracellular surfaces. In the voltage-sensor a relatively short proteinaceous region separates the inner from the outer cavity. Normally ions do not traverse the voltage-sensor; rather charged residues on the S4 segments (Arg or Lys) are transported from the inner crevice to the outer crevice during gating(Bezanilla, 2008). However, mutations of these charged S4 residues can induce “gating-pores” and “gating-pore currents” (Sokolov et al., 2005; Starace and Bezanilla, 2004; Struyk and Cannon, 2007; Tombola et al., 2007; Tombola et al., 2005). Importantly, these gating-pore currents are ionic currents that do not flow through the central pore of the channel but rather flow through the modified VGSC voltage-sensors (Figure 1C). The gating-pore currents generated by single charge mutations and carried by cations such as Na^+ and H^+ are $\leq$ 1% of the central pore current in VGSCs, but in potassium channels, because of their 4-fold symmetry, they can be larger (~6% of the central pore current) (Sokolov et al., 2005). Depending on which charged residues in the S4 segments

Downloaded from molpharm.aspetjournals.org at ASPET Journals on April 20, 2024

Molecular Pharmacology Fast Forward. Published on June 4, 2014 as DOI: 10.1124/mol.114.092338
This article has not been copyedited and formatted. The final version may differ from this version.

are mutated, gating-pore currents arise either in the resting or the activated configuration (Sokolov et al., 2007; Sokolov et al., 2008b) (Figure 1C). Monitoring gating pore currents can provide unique insight into the configuration of individual voltage sensors and how they respond to changes in transmembrane voltage.

We mutated the outer charged residues to induce inward gating-pore currents in the resting configuration. We show that inward gating-pore currents generated by each of the individual voltage-sensors can be measured from channels expressed in a mammalian cell line. We demonstrate that gating-pore currents can be used to precisely identify and monitor the ability of toxins to modulate the activity of the individual voltage-sensors.

Downloaded from molpharm.aspetjournals.org at ASPET Journals on April 20, 2024

Materials and Methods

Toxins

Anthopleurin B (ApB) was recombinantly produced as described by Gallagher and Blumenthal (Gallagher and Blumenthal, 1992). ProTx-II and huwentoxin-IV (HWTX-IV) were chemically synthesized as described by Middleton et al. (Middleton et al., 2002) and Xiao et al. (Xiao et al., 2008), respectively.

Plasmids and Construction of sodium channel Mutants

The cDNA genes encoding a TTX- and HWTX-IV-sensitive Nav1.5 (C373Y/R800D/S802E) and auxibiliary subunit β1 were cloned from human and subcloned into the pcDNA3.1 vector (Nav1.5) and an internal ribosome entry site vector (β1) (Lossin et al., 2002). All mutations inserted into the sodium channel cDNA gene were constructed using the QuickChange II XL Site-Directed Mutagenesis kit according to the manufacture's instruction. All constructs were sequenced to confirm that the appropriate mutations were made. The TTX- and HWTX-IV-sensitive modified wild-type Nav1.5 channel is referred to as WT* in this study.

Transient Transfection

Transient transfection of hNav1.5 constructs into human embryonic kidney 293 (HEK293) cells was performed using the calcium phosphate precipitation method. HEK293 cells were grown under standard tissue culture conditions (5% CO_2 and 37°C) in Dulbecco's modified Eagle's

Molecular Pharmacology Fast Forward. Published on June 4, 2014 as DOI: 10.1124/mol.114.092338
This article has not been copyedited and formatted. The final version may differ from this version.

medium supplemented with 10% fetal bovine serum (FBS). All hNav1.5 mutant channels were cotransfected with the hβ1 subunit to increase current density. The calcium phosphate-DNA mixture (channel constructs and a green fluorescent protein reporter plasmid) was added to the cell culture medium and left for 3 - 4 h, after which the cells were washed with fresh medium. Cells with green fluorescent protein fluorescence were selected for whole-cell patch-clamp recordings 36 to 72 h after transfection.

Electrophysiological Recordings

Ionic currents were recorded at room temperature (~21°C) using an EPC-10 amplifier and the Pulse program (version 8.31) (HEKA, Lambrecht/Pfalz, Germany). Fire-polished electrodes were fabricated from 1.7-mm capillary glass (VWR, West Chester, PA) using a P-97 puller (Sutter Instrument Company, Novato, CA). In order to minimize capacitive artifacts, the electrode tips were coated with sticky wax (KerrLab). After filling with the intracellular solution containing (in mM): CsF 140, EGTA 1.1, NaCl 10, and HEPES 10, pH 7.3 (adjusted with HCl), the access resistance of electrode pipettes ranged between 0.9 and 1.8 MΩ. The intracellular solution for recording outward gating pore current contained (in mM): CsF 130, Guanidine Sulfate 10 mM, EGTA 1.1, NaCl 10, and HEPES 10, pH 7.3 (adjusted with HCl). The bathing solution was (in mM): NaCl 140, $MgCl_2$ 1, $CaCl_2$ 3, and HEPES 10, pH 7.3 (adjusted with NaOH). The liquid junction potential for these solutions was <8 mV; data were not corrected to account for this offset. The offset potential was zeroed before patching. After establishing the whole-cell recording configuration, the cells were held at −100 mV for 5 min. A P/-5 subtraction protocol was used to remove linear leak current and capacitance artifact only for data shown in Figures 4A & B and 6A & B; no on-line subtraction was performed in other experiments. Ion currents were filtered at 5 kHz and sampled at 20 kHz. Voltage errors were minimized using 70 - 80% series resistance compensation.

Toxin stock solutions were made at 100 μM using the bathing solution containing 1 mg/ml bovine serum albumin, and aliquots were stored at −20°C. Before use, the solution was diluted to the concentrations of interest with fresh bathing solution. Toxin was diluted into the recording chamber (volume of 300 μl) and mixed by repeatedly pipetting 30 μl to achieve the specified final concentration.

Data Analysis

Data were analyzed using the software programs Pulsefit (HEKA) and GraphPad Prism 5.0 (GraphPad Software, Inc.). All data are shown as mean ± S.E. *n* is presented as the number of

Downloaded from molpharm.aspetjournals.org at ASPET Journals on April 20, 2024

Molecular Pharmacology Fast Forward. Published on June 4, 2014 as DOI: 10.1124/mol.114.092338
This article has not been copyedited and formatted. The final version may differ from this version.

the separate experimental cells. The “activation threshold” for gating pore currents (see figures 2, 3, 5 and 7) was defined as the most positive voltage where gating pore current can be observed above the baseline noise measured at fully depolarized potentials (i.e. 0 mV), and was judged by eye. Statistical analysis was carried out by Student's *t* test, and $p < 0.05$ indicated a significant difference.

Results

Quantification of sodium channel gating pore currents in mammalian cells

Our goal was to determine if gating pore currents could be used to investigate the mechanisms of interaction for toxins that modify VGSCs. Although gating pore currents have been observed in *Xenopus* oocytes, they have not previously been recorded from mammalian heterologous expression systems such as human embryonic kidney 293 (HEK293) cells. We used HEK293 cells here because voltage-gated ion channels may be more likely to undergo normal post-translational modifications in mammalian cells than in *Xenopus* oocytes, which could be an advantage in dissecting toxin-channel interactions.

We first determined if we could obtain measureable gating pore currents from each of the four individual voltage-sensors for a VGSC expressed in a mammalian cell line. In order to maximize our chances for success, we choose to use human Nav1.5 VGSCs, which routinely generate large central pore currents (often up to 50 nA) compared to other VGSCs. For our studies we used a hNav1.5 construct that was modified to be sensitive to the pore blocker tetrodotoxin (TTX) (Satin et al., 1992) and the gating modifier HWTX-IV (Xiao et al., 2008). Hereafter this hNav1.5-C373Y/R800D/S802E construct will be referred to as wild-type* (WT*) in order to distinguish it from the subsequent gating pore constructs containing additional mutations. In the WT* construct, 1 μM TTX blocked virtually all of the transient sodium current conducted by the central pore (Supplemental Figure 1A). In the presence of TTX, cells expressing WT* channels exhibited only linear leak currents; no gating pore currents were observed (Supplemental Figure 1B). To obtain measureable gating pore currents from each of

Downloaded from molpharm.aspetjournals.org at ASPET Journals on April 20, 2024

Molecular Pharmacology Fast Forward. Published on June 4, 2014 as DOI: 10.1124/mol.114.092338
This article has not been copyedited and formatted. The final version may differ from this version.

the individual voltage-sensors, we made a series of single, double and triple mutations in each domain where charged residues in the S4 segment (Figure 1B) were mutated to glycine residues. Although we were unable to reliably measure gating pore currents in HEK293 cells from channels with single mutations, mutating the first and second arginines in DI and DII to glycine (R1G/R2G) yielded resolvable gating pore currents at negative membrane potentials (Figure 2A). In order to obtain measureable gating pore currents from DIII and DIV, we found that it was necessary to mutate three charged residues in the S4 segments (K0G/R1G/R2G and R0G/R1G/R2G for DIII and DIV, respectively). For each of these constructs, the peak transient central pore current was blocked by the addition of TTX (Figure 2A, right panels). As was recently reported with Nav1.4 gating pore currents measured in *Xenopus* oocytes (Capes et al., 2012), TTX failed to alter the gating pore currents in the voltage-sensor subdomains of DI, DII and DIII, but slightly reduced the gating pore current amplitude of DIV ($p < 0.05$; Figure 2B). This is consistent with the notion that TTX can subtly impact the configuration of the DIV voltage-sensor. By contrast, the gating pore currents generated in each of the 4 voltage-sensors were substantially inhibited by 1 mM gadolinium (Supplemental Figure 2), consistent with previous studies in *Xenopus* oocytes (Sokolov et al., 2010). Interestingly, the voltage dependence of steady state inactivation was altered by charge mutations in DI, DIII and DIV, but not DII (Figure 2D). The amplitude of the gating pore currents, relative to the peak transient central pore current, generated by the different domains also differed significantly for the 4 voltage-sensors, with DII and DIV mutations generating the largest relative gating pore currents (Figure 2E).

Gating pore current analysis demonstrates that HWTX-IV selectively traps DII in the resting position

We next asked if gating pore currents could be used to characterize toxin-channel interactions. Previously we have used extensive site-directed mutagenesis to show that

Downloaded from molpharm.aspetjournals.org at ASPET Journals on April 20, 2024

Molecular Pharmacology Fast Forward. Published on June 4, 2014 as DOI: 10.1124/mol.114.092338
This article has not been copyedited and formatted. The final version may differ from this version.

tarantula toxin HWTX-IV inhibition of central pore currents critically depends on specific residues in the DII voltage-sensor(Xiao et al., 2008; Xiao et al., 2011), suggesting that HWTX-IV indirectly inhibited central pore currents by blocking movement of a voltage-sensor, and thus preventing activation of the channel. We examined the effects of HWTX-IV on inward gating pore currents generated by each of the 4 voltage-sensors and found that HWTX-IV only significantly altered the gating pore currents generated in DII (Figure 3A, B). HWTX-IV substantially enhanced the amplitude of the gating pore currents in DII and shifted the activation threshold for these inward DII gating pore currents by more than 50 mV in the depolarizing direction (Figure 3C). The modulation of DII gating pore currents by HWTX-IV was abolished by point mutations in the DII voltage-sensor (D800R/E802S) that also abolish the ability of HWTX-IV to inhibit the transient central pore currents (Figure 4) (Xiao et al., 2008). These data confirm that HWTX-IV specifically interacts with the DII voltage-sensor and provide compelling evidence that HWTX-IV inhibits central pore sodium currents by selectively trapping the DII voltage-sensor in the resting position, preventing channel activation.

Gating pore current analysis demonstrates that ApB selectively traps DIV in the resting position

We also examined the effect of the sea anemone toxin anthopleurin B (ApB) on the VGSC gating pore currents. ApB substantially enhances VGSC currents by selectively impairing fast inactivation (Benzinger et al., 1998). We found that ApB significantly enhanced the gating pore currents generated in DIV (Figure 5A, B), shifting the threshold for activation of the inward gating pore currents by almost +100 mV (Figure 5C), while having no effect on the gating pore currents generated by DI, DII and DIII. Because TTX also can impact DIV gating pore currents, we measured the effect of a saturating concentration of ApB on DIV gating pore currents in the absence and presence of TTX. The effects of ApB on DIV gating pore currents were observed in the absence and presence of TTX (Supplemental Figure 3), indicating that

Downloaded from molpharm.aspetjournals.org at ASPET Journals on April 20, 2024

Molecular Pharmacology Fast Forward. Published on June 4, 2014 as DOI: 10.1124/mol.114.092338
This article has not been copyedited and formatted. The final version may differ from this version.

while TTX can still bind to sodium channels in the presence of ApB, the impact of ApB on DIV gating pore currents dominates that of TTX. Site directed mutagenesis previously identified an aspartate residue (corresponding to D1610 in hNav1.5) in the extracellular portion of the DIV voltage-sensor that was crucial to ApB's ability to disrupt fast inactivation (Benzinger et al., 1998). The effects on DIV gating pore currents were abolished by the D1610R mutation that nearly eliminates the effect of ApB on sodium channel inactivation kinetics (Figure 6). Thus ApB impairs sodium current inactivation by selectively trapping the DIV voltage-sensor in the resting position.

ProTx-II has unique interactions with multiple sodium channel voltage-sensors

We next examined the effect of the tarantula toxin ProTx-II on VGSC gating pore currents. Although several studies have investigated the effects of ProTx-II on VGSCs, the details of the interaction remain unclear. ProTx-II can inhibit the central pore current of multiple VGSC isoforms (Middleton et al., 2002), but is most potent against Nav1.7 (Schmalhofer et al., 2008). Several studies have used site-directed mutagenesis to identify specific residues in the DII voltage-sensor that can partially reduce the inhibitory action of ProTx-II (Schmalhofer et al., 2008; Sokolov et al., 2008a), suggesting that in part ProTx-II inhibition may be due to trapping of the DII voltage-sensor in the closed state. However, extensive analyses of sodium channel chimeras have been unable to confirm the role of the DII voltage-sensor as the sole determinant of ProTx-II inhibition of Nav1.5, suggesting the toxin might interact with VGSCs in a novel manner (Smith et al., 2007). Paddle chimeras, where the S3-S4 linker of each VGSC domain was transplanted into a potassium channel, indicated that ProTx-II can interact with the voltage sensors in DI, DII and DIV (Bosmans et al., 2008). Previously we reported that ProTx-II could both inhibit the peak transient pore current of Nav1.7, in part by interacting with residues in the DII VSD, and impair inactivation of Nav1.7 through interactions with residues in DIV (Xiao et al., 2010). Here we show that ProTx-II significantly alters the gating pore currents generated by the DI, DII and DIV voltage-sensors (Figure 7). The impact on the DIV gating pore currents was

Downloaded from molpharm.aspetjournals.org at ASPET Journals on April 20, 2024

Molecular Pharmacology Fast Forward. Published on June 4, 2014 as DOI: 10.1124/mol.114.092338
This article has not been copyedited and formatted. The final version may differ from this version.

relatively minor but significant, which is consistent with our previous study indicating that the impairment of hNav1.5 inactivation by ProTx-II is ~50-fold less potent than the inhibitory effect on central pore current activation. However, ProTx-II is ~15-fold more potent at impairing inactivation of hNav1.7 than hNav1.5 DIV (Xiao et al., 2010). Therefore we asked if ProTx-II was able to inhibit hNav1.7 DIV gating pore current to a greater extent than that of hNav1.5, and this was indeed what we observed (Supplemental Figure 4).

ProTx-II had mixed effects on DII gating pore currents, inhibiting them at extreme negative potentials (< -180 mV) but substantially enhancing them between -160 and -10 mV. Surprisingly, ProTx-II substantially inhibited the gating-pore currents through the DI voltage sensor, suggesting that ProTx-II destabilizes the resting state of this voltage-sensor. To investigate this we created additional mutations in each of the hNav1.5 WT* voltage-sensors in an attempt to generate outward gating pore currents that would flow at depolarized potentials when the voltage-sensors were at activated positions (see schematic diagram in Figure 1C). We were unsuccessful in generating outward gating pore currents through the DIII and DIV voltage-sensors, but did obtain them in the DI and DII voltage-sensors after mutating the 3rd and 4th charged residues to glycine (Supplemental Figure 5). These outward gating pore currents were inhibited by 1 mM gadolinium (Supplemental Figure 6). Both ProTx-II and HWTX-IV substantially blocked the outward gating pore currents through the DII voltage-sensor (Figure 8C,D). This, in combination with the ability of both toxins to enhance inward gating pore currents in DII, is consistent with the proposal that these toxins both trap the DII voltage-sensor in the resting configuration. Protx-II also substantially blocked the outward gating pore currents generated in DI (Figure 8A), shifting the threshold for activation by +50 mV or more. Taken together, these data on ProTx-II effects on inward and outward gating pore currents indicate that ProTx-II does not trap the DI voltage-sensor in either the resting or activated configuration, but rather locks it in an intermediate state, preventing it from reaching the fully activated configuration. However, because ProTx-II may interact with both the DII and DIV voltage-

Downloaded from molpharm.aspetjournals.org at ASPET Journals on April 20, 2024

Molecular Pharmacology Fast Forward. Published on June 4, 2014 as DOI: 10.1124/mol.114.092338
This article has not been copyedited and formatted. The final version may differ from this version.

sensors, which flank the DI voltage-sensor, an alternative possibility was that ProTx-II only indirectly modifies the activity of the DI voltage-sensor. To test this possibility, we examined the effect of simultaneously applying both HWTX-IV and ApB on DI gating pore currents. In contrast to ProTx-II, co-application of HWTX-IV and ApB had only a minor inhibitory effect on the outward gating pore currents in DI (Figure 8B) and the inward gating pore currents generated by the R1G/R2G mutations in DI (Supplemental Figure 7). These data indicate that trapping both the DII and DIV voltage-sensors in the resting state has only a small impact on the movement of the DI voltage-sensor, and thus confirm that ProTx-II most probably blocks sodium channel activation by directly interacting with the DI as well as the DII voltage-sensor.

Downloaded from molpharm.aspetjournals.org at ASPET Journals on April 20, 2024

Discussion

VGSCs are intimately involved in normal and abnormal electrical excitability in a multitude of tissues. While numerous animal toxins and drugs can alter sodium currents and sodium channel gating, it is difficult to determine how specific agents alter the activity of individual sodium channel voltage-sensors. Here we used gating-pore currents to investigate the impact of three different peptide toxins on each of the four voltage-sensors. Our data show that 1) inward gating-pore currents, which reflect the resting configuration, can be recorded in HEK293 cells from each of the four voltage-sensors, 2) peptide toxins have unique signatures reflecting their interactions with the voltage-sensors, 3) the activity of the individual voltage sensors are independent and 4) the DIV voltage sensor plays a specialized role in channel activity. Overall these data demonstrate that gating-pore currents can be used to identify molecular determinants of sodium channel gating and pharmacology.

Although gating pore currents have previously been recorded from ion channels expressed in *Xenopus* oocytes, demonstration of gating pore current recordings from mammalian cell lines has been lacking. Here we demonstrated that inward gating pore currents can be recorded from each of the 4 voltage-sensors following sodium channel expression in

Molecular Pharmacology Fast Forward. Published on June 4, 2014 as DOI: 10.1124/mol.114.092338
This article has not been copyedited and formatted. The final version may differ from this version.

HEK293 cells. Outward gating pore currents could be recorded from DI and DII voltage sensors. Although the gating pore currents are smaller in mammalian cell lines and thus more challenging to record, heterologous expression of sodium channels in mammalian cell lines can have advantages. Post-translational modifications are more likely to be conserved and therefore gating and pharmacological properties should better replicate those of sodium channels in primary cells. In addition, mammalian cell lines such as HEK293 cells are more amenable to screening assays. Because gating pore currents provide a more direct measurement of the conformation changes that individual voltage-sensors undergo, and because they have the potential to substantially alter resting membrane potential and proton flux (Wu et al., 2011), gating pore current constructs may eventually be useful in high throughput fluorescent screening assays for gating modifiers. However, one caveat of the approach is that it requires mutating charged residues in the S4 segments. Although mutating the outer S4 arginine residues in DII did not significantly alter sodium channel inhibition by HWTX-IV (Xiao et al., 2011) or ProTx-II (Sokolov et al., 2008a), arginine mutations can impact some toxin channel interactions (Bosmans et al., 2008) and this potential influence needs to be considered.

Our data showed that HWTX-IV selectively enhanced inward gating pore currents generated in the DII voltage-sensor. This is consistent with HWTX-IV selectively trapping the DII voltage-sensor in the closed configuration. Although HWTX-IV can fully inhibit central pore currents, it is interesting to note that HWTX-IV had no effect on the amplitude or voltage-dependence of gating pore currents generated in the other three voltage-sensors. Thus trapping the DII voltage-sensor in the closed configuration is sufficient to prevent activation. Interestingly, HWTX-IV did not simply shift the voltage-dependence of the DII gating pore currents, but also seemingly enhanced the amplitude at negative potentials. This suggests that even at -200 mV, the voltage-sensor in the absence of toxin is not fully locked in the closed position, but fluctuates between configurations that do and do not allow the flow of gating pore currents. One possibility is that HWTX-IV enhances gating pore current amplitude by stabilizing

Downloaded from molpharm.aspetjournals.org at ASPET Journals on April 20, 2024

Molecular Pharmacology Fast Forward. Published on June 4, 2014 as DOI: 10.1124/mol.114.092338
This article has not been copyedited and formatted. The final version may differ from this version.

the voltage-sensor in a position that permits a more consistent flow of ions through the gating pore. Alternative explanations include the possibility that the toxin binding alters the size of the gating pore, thus enhancing ion flow. It is difficult to determine the precise mechanism underlying the increased gating pore current amplitude based on our data presented here.

ApB selectively enhanced inward gating pore currents generated in the DIV voltage-sensor. This is consistent with ApB selectively trapping the DIV voltage-sensor in the closed configuration. However, ApB does not inhibit central pore currents but rather selectively impairs open channel inactivation. Thus selectively trapping the DIV voltage-sensor in the closed configuration does not prevent the other voltage-sensors from shifting to the outward, activated configuration and inducing opening of the channel pore. Taken together these data demonstrate that the activity of the four voltage-sensors is essentially independent and that while activation of the DII voltage-sensor is crucial for opening the sodium channel central pore, activation of the DIV voltage sensor is not necessary. This demonstration that the DIV voltage sensor plays a crucial and selective role in open-channel inactivation is at odds with the proposal that inactivation does not have inherent voltage-dependence (Aldrich et al., 1983; Bezanilla and Armstrong, 1977), but consistent with more recent studies suggesting the DIV voltage-sensor has a unique specialized role in inactivation (Capes et al., 2013; Chen et al., 1996; Sheets et al., 1999; Yang and Kuo, 2003).

ProTx-II has complex actions on VGSC currents (Edgerton et al., 2008) and the molecular determinants of these actions have been elusive and controversial (Bosmans et al., 2008; Bosmans et al., 2006; Schmalhofer et al., 2008; Smith et al., 2007; Sokolov et al., 2008a; Xiao et al., 2010). Our data show that ProTx-II substantially modulates the conformation of both the DI and DII voltage sensors in Nav1.5. Although ProTx-II predominantly enhanced inward gating pore currents generated in DII, indicating that it favors the resting configuration of this voltage sensor, it inhibited inward gating pore currents generated in DI, suggesting that it stabilizes the DI voltage-sensors into an intermediate configuration. ProTx-II is considered

Downloaded from molpharm.aspetjournals.org at ASPET Journals on April 20, 2024

Molecular Pharmacology Fast Forward. Published on June 4, 2014 as DOI: 10.1124/mol.114.092338
This article has not been copyedited and formatted. The final version may differ from this version.

highly lipophillic and likely inserts into the membrane in order to interact with VGSCs (Smith et al., 2005). It is interesting to note that binding studies suggest that there may only be one high affinity ProTx-II binding site on Nav1.7 channels (Schmalhofer et al., 2008). These observations raise the intriguing possibility that a single ProTx-II molecule might simultaneously interact with the DI and DII voltage-sensors in a novel manner compared to that of other VGSC gating modifiers. Although the tarantula toxins HWTX-IV and ProTx-II can both inhibit sodium channel central pore currents and interact with the DII voltage-sensor, our gating pore current data, in conjunction with mutagenesis studies (Bosmans et al., 2008; Schmalhofer et al., 2008; Xiao et al., 2008; Xiao et al., 2010) indicate that these two peptide toxins have distinct interactions with voltage-gated sodium channels.

Overall, our data demonstrate that gating pore currents can provide unique insight into the ability of toxins to impact the activity of individual voltage-sensors and help identify the molecular determinants of toxin-channel interactions. The gating pore current analysis approach that we developed could also be used to explore the mechanism of action of small molecules that target voltage-gated sodium channels. Furthermore, we expect that gating pore currents could be used to investigate of the molecular pharmacology of other voltage-gated ion channels (e.g., TRP channels, calcium channels, potassium channels) as well.

Downloaded from molpharm.aspetjournals.org at ASPET Journals on April 20, 2024

Molecular Pharmacology Fast Forward. Published on June 4, 2014 as DOI: 10.1124/mol.114.092338
This article has not been copyedited and formatted. The final version may differ from this version.

Authors Contributions

Participated in research design: Xiao, Blumenthal and Cummins.
Conducted experiments: Xiao.
Contributed new reagents or analytic tools: Xiao.
Performed data analysis: Xiao and Cummins.
Wrote or contributed to the writing of the manuscript: Xiao, Blumenthal and Cummins.

Downloaded from molpharm.aspetjournals.org at ASPET Journals on April 20, 2024

Molecular Pharmacology Fast Forward. Published on June 4, 2014 as DOI: 10.1124/mol.114.092338
This article has not been copyedited and formatted. The final version may differ from this version.

References

Aldrich RW, Corey DP and Stevens CF (1983) A reinterpretation of mammalian sodium channel gating based on single channel recording. *Nature* **306**(5942): 436-441.

Benzinger GR, Kyle JW, Blumenthal KM and Hanck DA (1998) A specific interaction between the cardiac sodium channel and site-3 toxin anthopleurin B. *J Biol Chem* **273**(1): 80-84.

Bezanilla F (2008) How membrane proteins sense voltage. *Nat Rev Mol Cell Biol* **9**(4): 323-332.

Bezanilla F and Armstrong CM (1977) Inactivation of the sodium channel. I. Sodium current experiments. *J Gen Physiol* **70**(5): 549-566.

Blumenthal KM and Seibert AL (2003) Voltage-gated sodium channel toxins: poisons, probes, and future promise. *Cell Biochem Biophys* **38**(2): 215-238.

Bosmans F, Martin-Eauclaire MF and Swartz KJ (2008) Deconstructing voltage sensor function and pharmacology in sodium channels. *Nature* **456**(7219): 202-208.

Bosmans F, Rash L, Zhu S, Diochot S, Lazdunski M, Escoubas P and Tytgat J (2006) Four novel tarantula toxins as selective modulators of voltage-gated sodium channel subtypes. *Mol Pharmacol* **69**(2): 419-429.

Capes DL, Arcisio-Miranda M, Jarecki BW, French RJ and Chanda B (2012) Gating transitions in the selectivity filter region of a sodium channel are coupled to the domain IV voltage sensor. *Proc Natl Acad Sci U S A* **109**(7): 2648-2653.

Capes DL, Goldschen-Ohm MP, Arcisio-Miranda M, Bezanilla F and Chanda B (2013) Domain IV voltage-sensor movement is both sufficient and rate limiting for fast inactivation in sodium channels. *J Gen Physiol* **142**(2): 101-112.

Catterall WA (2002) Molecular mechanisms of gating and drug block of sodium channels. *Novartis Found Symp* **241**: 206-218.

Cestele S and Catterall WA (2000) Molecular mechanisms of neurotoxin action on voltage-gated sodium channels. *Biochimie* **82**(9-10): 883-892.

Chen LQ, Santarelli V, Horn R and Kallen RG (1996) A unique role for the S4 segment of domain 4 in the inactivation of sodium channels. *J Gen Physiol* **108**(6): 549-556.

Edgerton GB, Blumenthal KM and Hanck DA (2008) Evidence for multiple effects of ProTxII on activation gating in Na(V)1.5. *Toxicon* **52**(3): 489-500.

Gallagher MJ and Blumenthal KM (1992) Cloning and expression of wild-type and mutant forms of the cardiotonic polypeptide anthopleurin B. *J Biol Chem* **267**(20): 13958-13963.

George AL, Jr. (2005) Inherited disorders of voltage-gated sodium channels. *J Clin Invest* **115**(8): 1990-1999.

Lossin C, Wang DW, Rhodes TH, Vanoye CG and George AL, Jr. (2002) Molecular basis of an inherited epilepsy. *Neuron* **34**(6): 877-884.

Middleton RE, Warren VA, Kraus RL, Hwang JC, Liu CJ, Dai G, Brochu RM, Kohler MG, Gao YD, Garsky VM, Bogusky MJ, Mehl JT, Cohen CJ and Smith MM (2002) Two tarantula peptides inhibit activation of multiple sodium channels. *Biochemistry* **41**(50): 14734-14747.

Satin J, Kyle JW, Chen M, Bell P, Cribbs LL, Fozzard HA and Rogart RB (1992) A mutant of TTX-resistant cardiac sodium channels with TTX-sensitive properties. *Science* **256**(5060): 1202-1205.

Schmalhofer WA, Calhoun J, Burrows R, Bailey T, Kohler MG, Weinglass AB, Kaczorowski GJ, Garcia ML, Koltzenburg M and Priest BT (2008) ProTx-II, a selective inhibitor of NaV1.7 sodium channels, blocks action potential propagation in nociceptors. *Mol Pharmacol* **74**(5): 1476-1484.

Sheets MF, Kyle JW, Kallen RG and Hanck DA (1999) The Na channel voltage sensor associated with inactivation is localized to the external charged residues of domain IV, S4. *Biophys J* **77**(2): 747-757.

Downloaded from molpharm.aspetjournals.org at ASPET Journals on April 20, 2024

Molecular Pharmacology Fast Forward. Published on June 4, 2014 as DOI: 10.1124/mol.114.092338
This article has not been copyedited and formatted. The final version may differ from this version.

Smith JJ, Alphy S, Seibert AL and Blumenthal KM (2005) Differential phospholipid binding by site 3 and site 4 toxins. Implications for structural variability between voltage-sensitive sodium channel domains. *J Biol Chem* **280**(12): 11127-11133.

Smith JJ, Cummins TR, Alphy S and Blumenthal KM (2007) Molecular interactions of the gating modifier toxin ProTx-II with NaV 1.5: implied existence of a novel toxin binding site coupled to activation. *J Biol Chem* **282**(17): 12687-12697.

Sokolov S, Kraus RL, Scheuer T and Catterall WA (2008a) Inhibition of sodium channel gating by trapping the domain II voltage sensor with protoxin II. *Mol Pharmacol* **73**(3): 1020-1028.

Sokolov S, Scheuer T and Catterall WA (2005) Ion permeation through a voltage- sensitive gating pore in brain sodium channels having voltage sensor mutations. *Neuron* **47**(2): 183-189.

Sokolov S, Scheuer T and Catterall WA (2007) Gating pore current in an inherited ion channelopathy. *Nature* **446**(7131): 76-78.

Sokolov S, Scheuer T and Catterall WA (2008b) Depolarization-activated gating pore current conducted by mutant sodium channels in potassium-sensitive normokalemic periodic paralysis. *Proc Natl Acad Sci U S A* **105**(50): 19980-19985.

Sokolov S, Scheuer T and Catterall WA (2010) Ion permeation and block of the gating pore in the voltage sensor of NaV1.4 channels with hypokalemic periodic paralysis mutations. *J Gen Physiol* **136**(2): 225-236.

Starace DM and Bezanilla F (2004) A proton pore in a potassium channel voltage sensor reveals a focused electric field. *Nature* **427**(6974): 548-553.

Struyk AF and Cannon SC (2007) A Na+ channel mutation linked to hypokalemic periodic paralysis exposes a proton-selective gating pore. *J Gen Physiol* **130**(1): 11-20.

Tombola F, Pathak MM, Gorostiza P and Isacoff EY (2007) The twisted ion-permeation pathway of a resting voltage-sensing domain. *Nature* **445**(7127): 546-549.

Tombola F, Pathak MM and Isacoff EY (2005) Voltage-sensing arginines in a potassium channel permeate and occlude cation-selective pores. *Neuron* **45**(3): 379-388.

Waxman SG, Dib-Hajj S, Cummins TR and Black JA (2000) Sodium channels and their genes: dynamic expression in the normal nervous system, dysregulation in disease states(1). *Brain Res* **886**(1-2): 5-14.

Wu F, Mi W, Burns DK, Fu Y, Gray HF, Struyk AF and Cannon SC (2011) A sodium channel knockin mutant (NaV1.4-R669H) mouse model of hypokalemic periodic paralysis. *J Clin Invest* **121**(10): 4082-4094.

Xiao Y, Bingham JP, Zhu W, Moczydlowski E, Liang S and Cummins TR (2008) Tarantula huwentoxin-IV inhibits neuronal sodium channels by binding to receptor site 4 and trapping the domain II voltage sensor in the closed configuration. *J Biol Chem*. **283**(40): 27300-27313.

Xiao Y, Blumenthal K, Jackson JO, 2nd, Liang S and Cummins TR (2010) The tarantula toxins ProTx-II and huwentoxin-IV differentially interact with human Nav1.7 voltage sensors to inhibit channel activation and inactivation. *Mol Pharmacol* **78**(6): 1124-1134.

Xiao Y, Jackson JO, 2nd, Liang S and Cummins TR (2011) Common molecular determinants of tarantula huwentoxin-IV inhibition of Na+ channel voltage sensors in domains II and IV. *J Biol Chem* **286**(31): 27301-27310.

Yang YC and Kuo CC (2003) The position of the fourth segment of domain 4 determines status of the inactivation gate in Na+ channels. *J Neurosci* **23**(12): 4922-4930.

Downloaded from molpharm.aspetjournals.org at ASPET Journals on April 20, 2024

Molecular Pharmacology Fast Forward. Published on June 4, 2014 as DOI: 10.1124/mol.114.092338
This article has not been copyedited and formatted. The final version may differ from this version.

Footnotes

This work was supported by a grant from the National Institutes of Health National Institute of Neurological Disorders and Stroke [NS077805] to T.R.C.

Downloaded from molpharm.aspetjournals.org at ASPET Journals on April 20, 2024

Molecular Pharmacology Fast Forward. Published on June 4, 2014 as DOI: 10.1124/mol.114.092338
This article has not been copyedited and formatted. The final version may differ from this version.

Legends for Figures

Figure 1. Diagrams of voltage gated sodium channels. (A), Schematic diagram of sodium channel α subunit Nav1.5 (*Upper*). The voltage sensor (S4 segment) of each domain is shaded in *grey* and marked with "++". The α subunit contains three mutation sites: C373Y (filled circle), TTX-sensitive; R800D (filled diamond) and S802E (filled pentagon): HWTX-IV-sensitive. (B), The amino acid sequences of four S4 segments are aligned. The gating charge residues (Lys/Arg) are highlighted in blue and the numbering scheme for these residues is shown below. (C), Schematic diagram depicting channel central pore current (left panel), inward gating pore current with central pore current blocked (middle panel) and outward gating pore current with central pore current blocked (right panel).

Figure 2. Inward Igp were generated by mutations of the charged residues in the individual DI-DIV voltage sensors of Nav1.5. (A), Typical Current traces before (*left*) and after (*right*) 1 μM TTX treatment were elicited by 100-ms hyperpolarizing steps to various potentials that ranged from -200 to +40 mV in a 10-mV increment. The cells were held at -100 mV. The dotted line represents the zero current level. Linear leak and capacitance currents were not subtracted. (B) Effects of TTX on the current-voltage (I-V) curves of inward Igp. The subtraction of linear leak currents has been performed in the absence (filled circles) or presence (open circles) of 1 μM TTX. Igp were normalized to the maximal control Igp. (C), Activation threshold of Igp through the four voltage sensors measured in the presence of TTX. (D), Effects of Gly-mutations of gating-charge residues in four S4 segments on steady-state inactivation. The voltage dependence of steady-state inactivation was estimated using a standard double pulse protocol. Currents were plotted as a fraction of the maximal peak current. Data points were fitted with a standard Boltzmann equation. (E), Ratio of Igp to the total central pore current (I_{Na}). I_{Na} was estimated by the equation: $I_{Na} = I_{-100}/hinf_{-100}$, in which I_{-100} is the maximal central pore

Downloaded from molpharm.aspetjournals.org at ASPET Journals on April 20, 2024

Molecular Pharmacology Fast Forward. Published on June 4, 2014 as DOI: 10.1124/mol.114.092338
This article has not been copyedited and formatted. The final version may differ from this version.

current when cells were held at -100 mV, and $hinf_{-100}$ is the fraction of the total sodium channels available at -100 mV based on steady-state inactivation curve as shown in (D). *, $P < 0.05$; #, $P < 0.01$.

Figure 3. Effect of HWTX-IV on inward Igp generated by DI-DIV voltage-sensor mutants. (A) Typical inward hNav1.5 Igp current traces before and after 1 μM HWTX-IV treatment are shown. Cells were held at -100 mV and pretreated with 1 μM TTX. Currents before (left) and after (right) toxin treatment were elicited by 100-ms hyperpolarizing steps to various potentials that ranged from -200 mV to +40 mV in a 10-mV increment. The dotted line across current traces represents the zero current level. Linear leak and capacitance currents were not subtracted. (B) shows the effect of HWTX-IV on the I-V curves of inward Igp. In the I-V curves, the subtraction of linear leak currents has been performed before (filled circles) and after application (open circles) of 1 μM HWTX-IV. Igp were normalized to the maximal control Igp. (C) shows the effect of HWTX-IV on the activation threshold of Igp fluxing through four voltage sensors, respectively. N.S., no significance; *, $P < 0.05$; #, $P < 0.01$.

Figure 4. The double mutation (D800R/E802S) abolished the ability of HWTX-IV to alter the inward Igp fluxing through DII voltage sensor mutant. (A), Effects of HWTX-IV on the central pore currents from the WT* and double mutant R800D/S802E Nav1.5 channels. Current traces before (*black*) and after (*grey*) 1 μM HWTX-IV treatment were induced by a 20-ms depolarizing potential of -10 mV from a holding potential of -100 mV. (B), Fraction of remaining currents in the presence of 1 μM HWTX-IV. (C), HWTX-IV positively shifted the I-V curve of the inward Igp generated by hNav1.5 DII voltage sensor mutant (R1G/R2G). (D), double mutation D800R/E802S abolished the effect of HWTX-IV on the inward Igp generated by DII voltage sensor mutant (R1G/R2G). In both (C) and (D), Igp were elicited by the protocol as described in the legend of Supplemental Figure 3. Cells were held at -100 mV and pretreated with 1 μM TTX.

Downloaded from molpharm.aspetjournals.org at ASPET Journals on April 20, 2024

Molecular Pharmacology Fast Forward. Published on June 4, 2014 as DOI: 10.1124/mol.114.092338
This article has not been copyedited and formatted. The final version may differ from this version.

All currents are normalized to the maximal control current amplitude. Linear leak currents were subtracted.

Figure 5. Effect of ApB on inward Igp generated by DI-DIV voltage-sensor mutants. (A) Typical inward hNav1.5 Igp current traces before and after 100 nM ApB treatment are shown. Cells were held at -100 mV and pretreated with 1 μM TTX. Currents before (left) and after (right) toxin treatment were elicited by the protocol as described in the legend of Figure 3. The dotted line across current traces represents the zero current level. No linear leak and capacitance currents were subtracted. (B) shows the effect of ApB on the I-V curves of inward Igp. In all I-V curves, the subtraction of linear leak currents has been performed before (filled circles) and after application (open circles) of 100 nM ApB. Igp were normalized to the maximal control Igp. (C) shows the effect of ApB on the activation threshold of Igp fluxing through four voltage sensors, respectively. N.S., no significance; *, $P < 0.05$; #, $P < 0.01$.

Figure 6. The D1610R mutation significantly reduced the sensitivity of Nav1.5 to ApB. (A), The D1610R mutation decreased the ability of ApB to slow fast-inactivation of Nav1.5. Current traces before (*black* lines) and after (*grey* lines) application of 100 nM ApB were induced by a 20-ms depolarizing potential of -10 mV from a holding potential of -100 mV. (B), The ratio of I_{5ms} to peak current in the presence of 100 nM ApB. I_{5ms} was shown as the current not inactivated at 5 ms in (A). (C), ApB positively shifted the I-V curve of Igp fluxing through hNav1.5 DIV voltage sensor mutant. (D), Single mutation D1610R abolished ApB sensitivity of DIV inward Igp. In both (C) and (D), Igp were elicited by the protocol as described in the legend of Supplemental Figure 3. The subtraction of linear leak currents has been performed. Cells were held at -100 mV and pretreated with 1 μM TTX. All currents are normalized to the maximal control current amplitude. ApB concentration is 100 nM. Note that WT* means the triple C373Y/R800D/S802E mutant Nav1.5 channel.

Downloaded from molpharm.aspetjournals.org at ASPET Journals on April 20, 2024

Molecular Pharmacology Fast Forward. Published on June 4, 2014 as DOI: 10.1124/mol.114.092338
This article has not been copyedited and formatted. The final version may differ from this version.

Figure 7. Effect of ProTx-II on inward Igp generated by DI-DIV voltage-sensor mutants. Cells were held at -100 mV and pretreated with 1 μM TTX. Currents before (left) and after (right) 1 μM ProTx-II treatment were elicited by 100-ms hyperpolarizing steps to various potentials that ranged from -200 mV to +40 mV in a 10-mV increment. (A-D) show the effects of ProTx-II on the I-V curves of inward Igp for the DI-DIV voltage-sensors, respectively. In all I-V curves, the subtraction of linear leak currents has been performed before (filled circles) and after application (open circles) of 1 μM ProTx-II. Igp were normalized to the maximal control Igp. (E) shows the effect of ProTx-II on the activation threshold of Igp fluxing through four voltage sensors, respectively. N.S., no significance; *, $P < 0.05$; #, $P < 0.01$.

Figure 8. Effects of toxins on outward Igp fluxing through Nav1.5. Typical outward Igp current traces and associated I-V curves before and after toxin treatment are shown. (A), Effect of ProTx-II on DI outward Igp. (B), Effect of the mixture of ApB (100 nM) and HWTX-IV (1 μM) on DI outward Igp. (C), Effect of ProTx-II on DII outward Igp. (D), Effect of HWTX-IV on DII outward Igp. All currents before (*left*) and after (*right*) toxin treatment were elicited by 100-ms depolarizing steps to various potentials that ranged from -100 to +70 mV. No subtraction of linear leak and capacitance currents was performed for current traces. The dotted line across current traces represents the zero current level. Cells were pretreated with 1 μM TTX to completely block the central pore current and held at -100 mV. Note that in the I-V curves, linear leak currents have been subtracted. *, $P < 0.05$; # < 0.01.

Downloaded from molpharm.aspetjournals.org at ASPET Journals on April 20, 2024

Figure 1

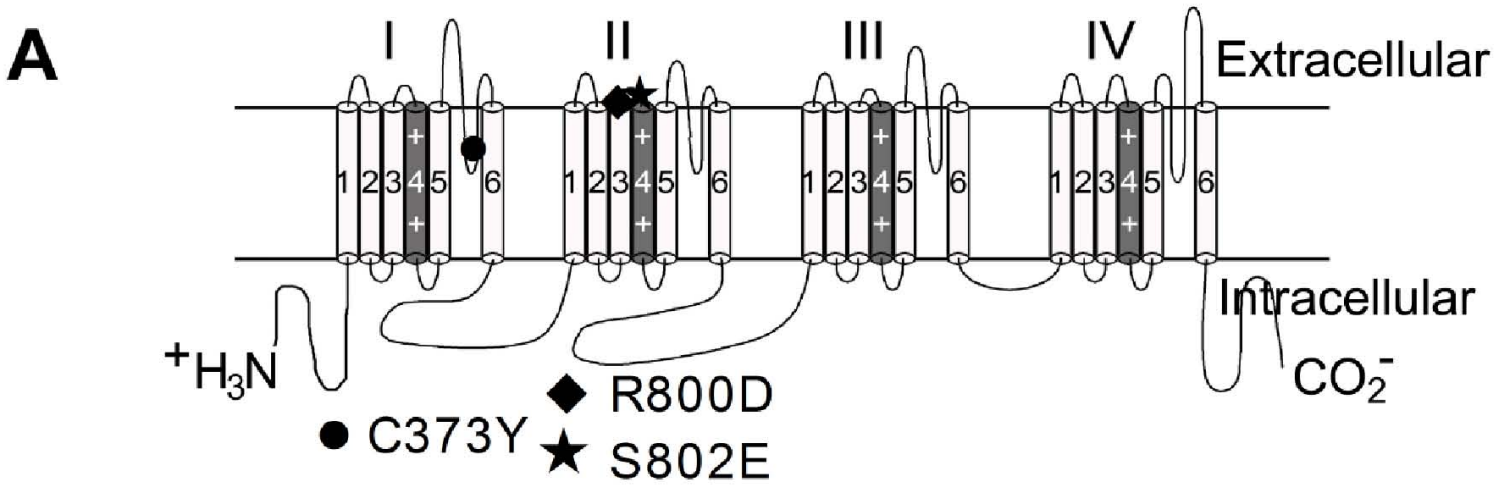
A
I
II
III
IV
Extracellular
Intracellular
1 2 3 4 5 6
+H3N
CO2-
R800D
C373Y
S802E

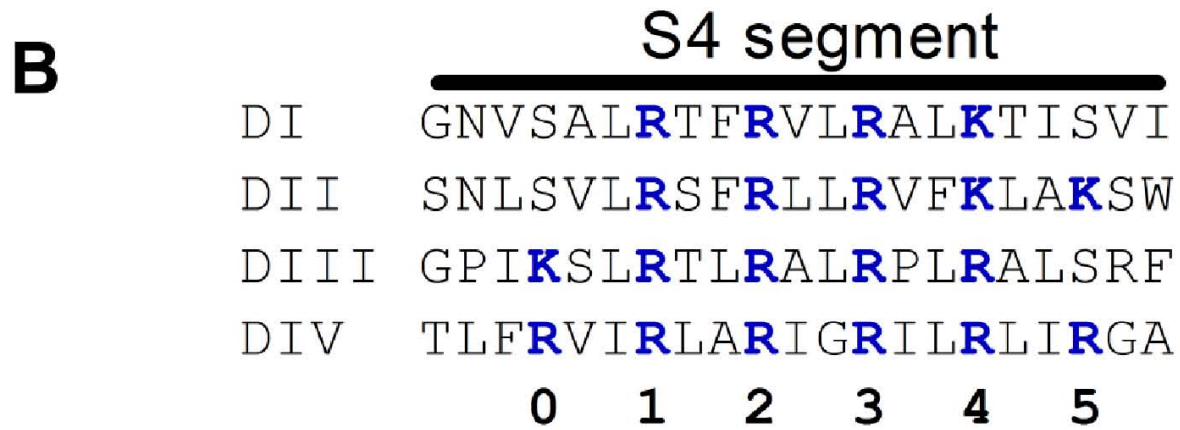
B
S4 segment
DI GNVSALRTFRVLRALKTISVI
DII SNLSVLRSFRLLRVFKLAKSW
DIII GPIKSLRTLRALRPLRALSRF
DIV TLFRVIRLARIGRILRLIRGA
0 1 2 3 4 5

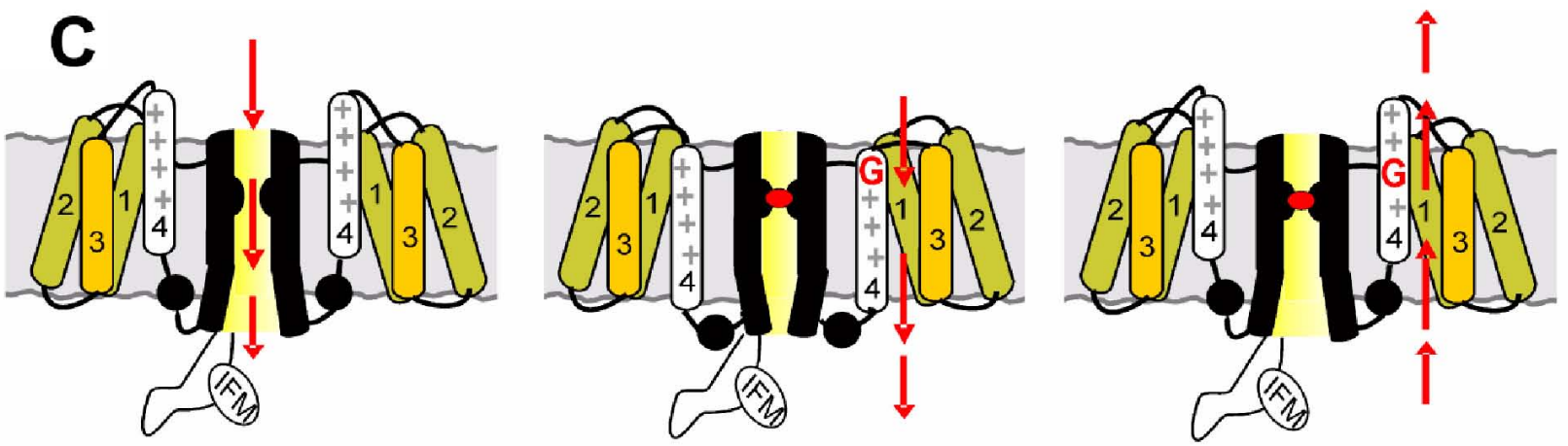
C
IFM
G
central pore current
inward gating pore current
outward gating pore current

Figure 2

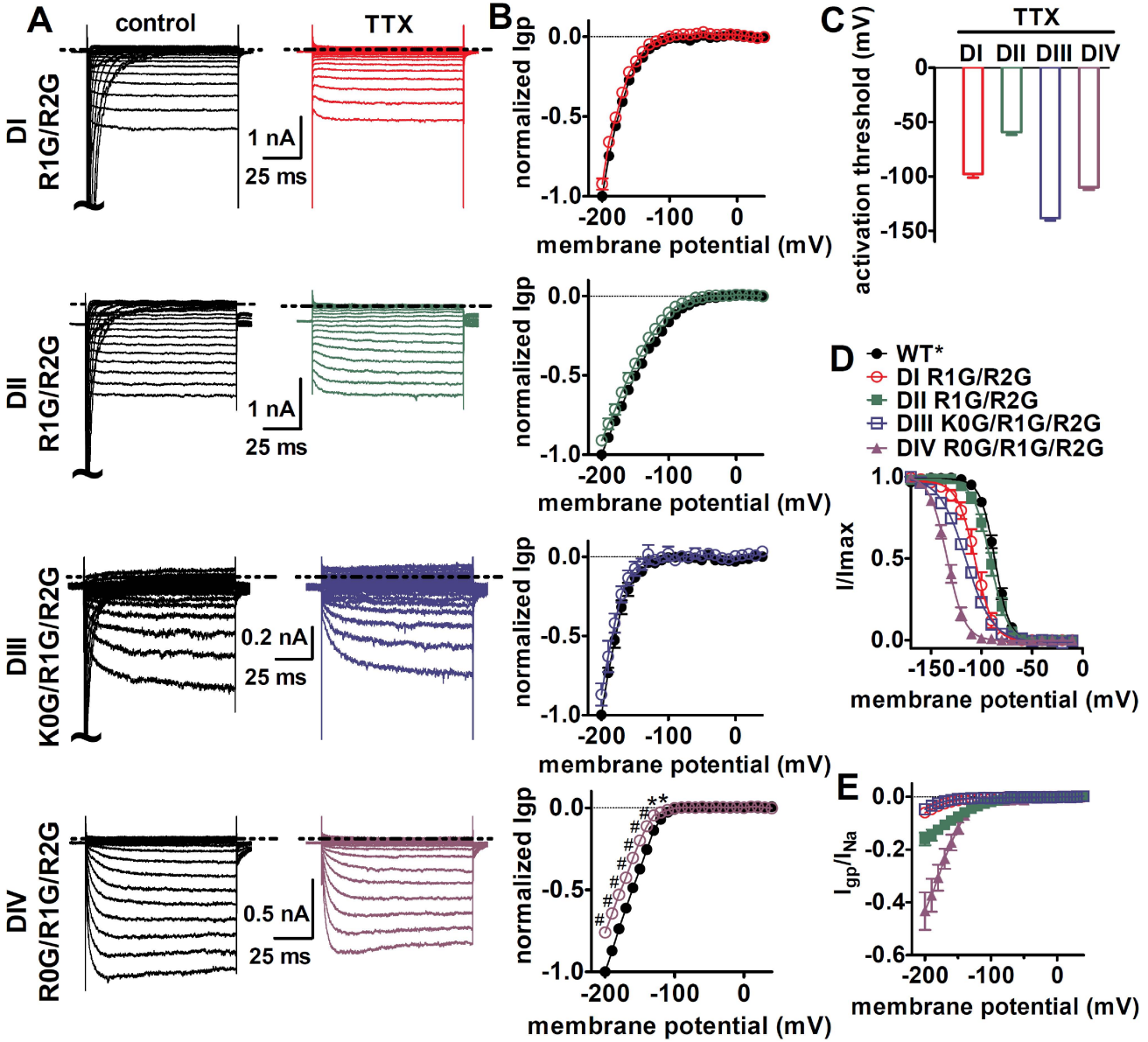
A
control
TTX
DI
R1G/R2G
1 nA
25 ms
DII
R1G/R2G
1 nA
25 ms
DIII
K0G/R1G/R2G
0.2 nA
25 ms
DIV
R0G/R1G/R2G
0.5 nA
25 ms
B
normalized Igp
membrane potential (mV)
C
TTX
DI DII DIII DIV
activation threshold (mV)
D
WT*
DI R1G/R2G
DII R1G/R2G
DIII K0G/R1G/R2G
DIV R0G/R1G/R2G
I/Imax
membrane potential (mV)
E
Igp/INa
membrane potential (mV)

Figure 3

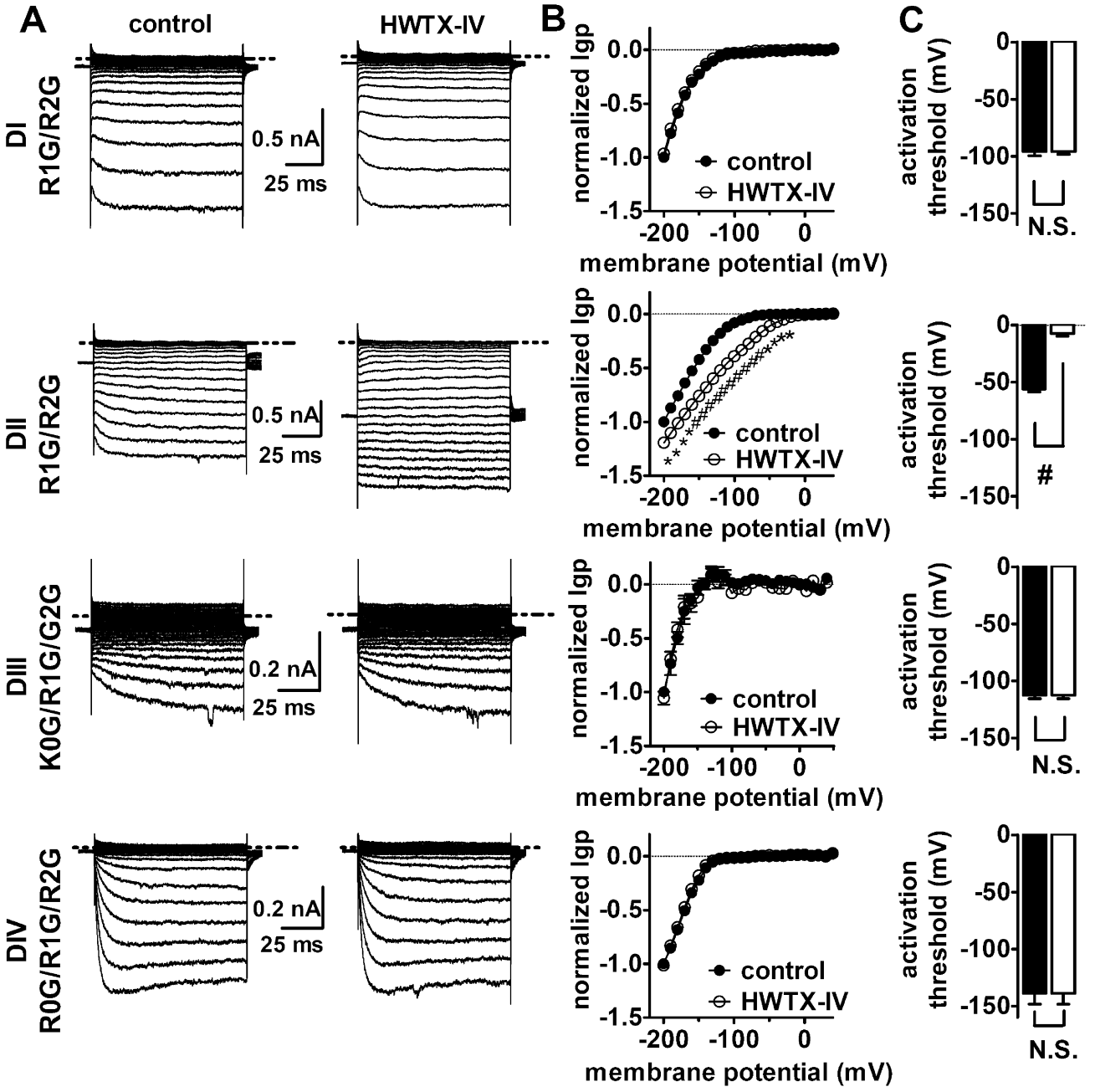
A
control
HWTX-IV
B
C
DI
R1G/R2G
0.5 nA
25 ms
normalized Igp
0.0
-0.5
-1.0
-1.5
control
HWTX-IV
-200
-100
0
membrane potential (mV)
activation threshold (mV)
0
-50
-100
-150
N.S.
DII
R1G/R2G
0.5 nA
25 ms
control
HWTX-IV
membrane potential (mV)
#
DIII
K0G/R1G/G2G
0.2 nA
25 ms
control
HWTX-IV
membrane potential (mV)
N.S.
DIV
R0G/R1G/R2G
0.2 nA
25 ms
control
HWTX-IV
membrane potential (mV)
N.S.

Figure 4

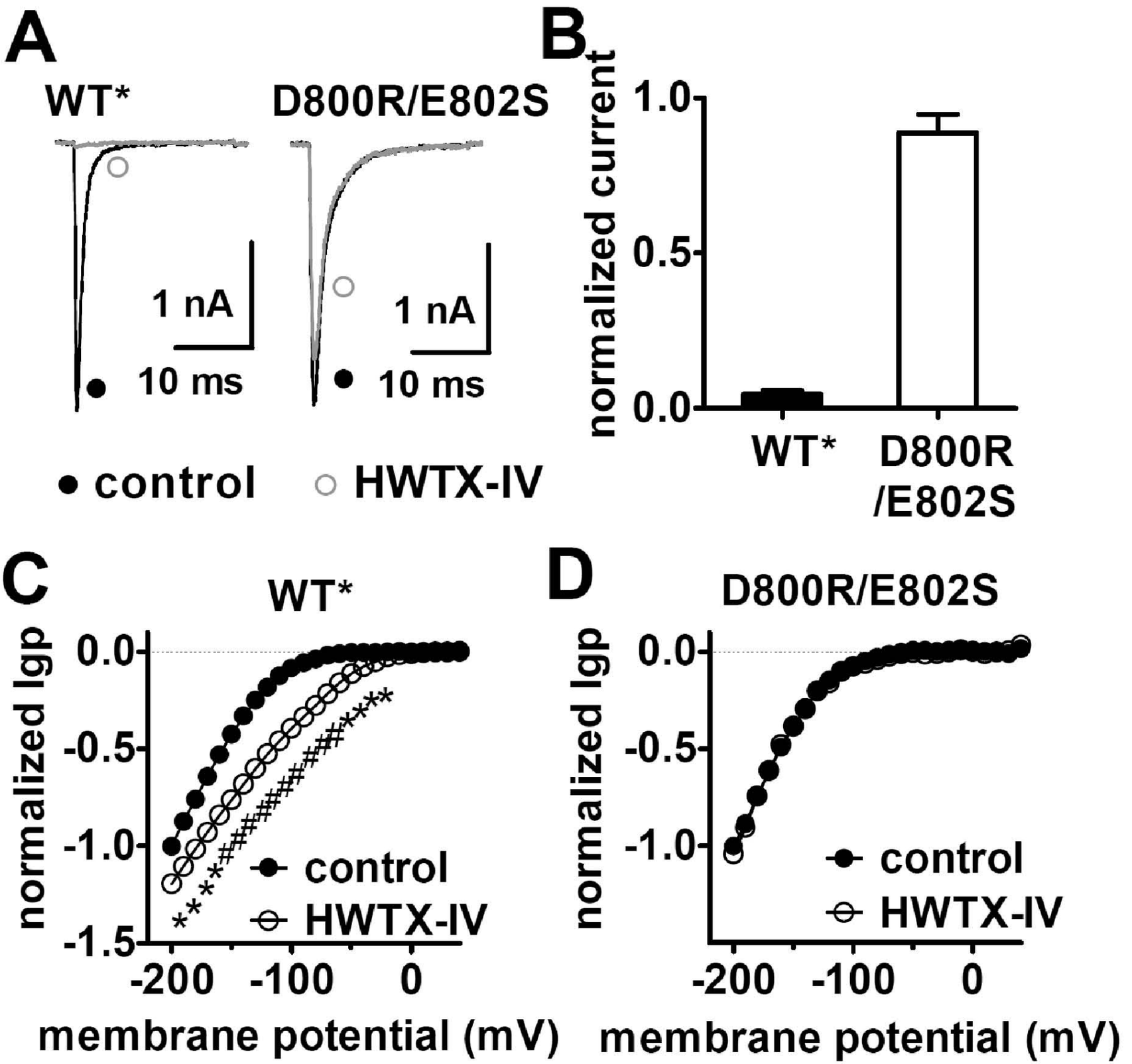
A
WT*
D800R/E802S
1 nA
10 ms
1 nA
10 ms
control
HWTX-IV
B
normalized current
1.0
0.5
0.0
WT*
D800R
/E802S
C
WT*
normalized Igp
0.0
-0.5
-1.0
-1.5
control
HWTX-IV
-200
-100
0
membrane potential (mV)
D
D800R/E802S
normalized Igp
0.0
-0.5
-1.0
control
HWTX-IV
-200
-100
0
membrane potential (mV)

Figure 5

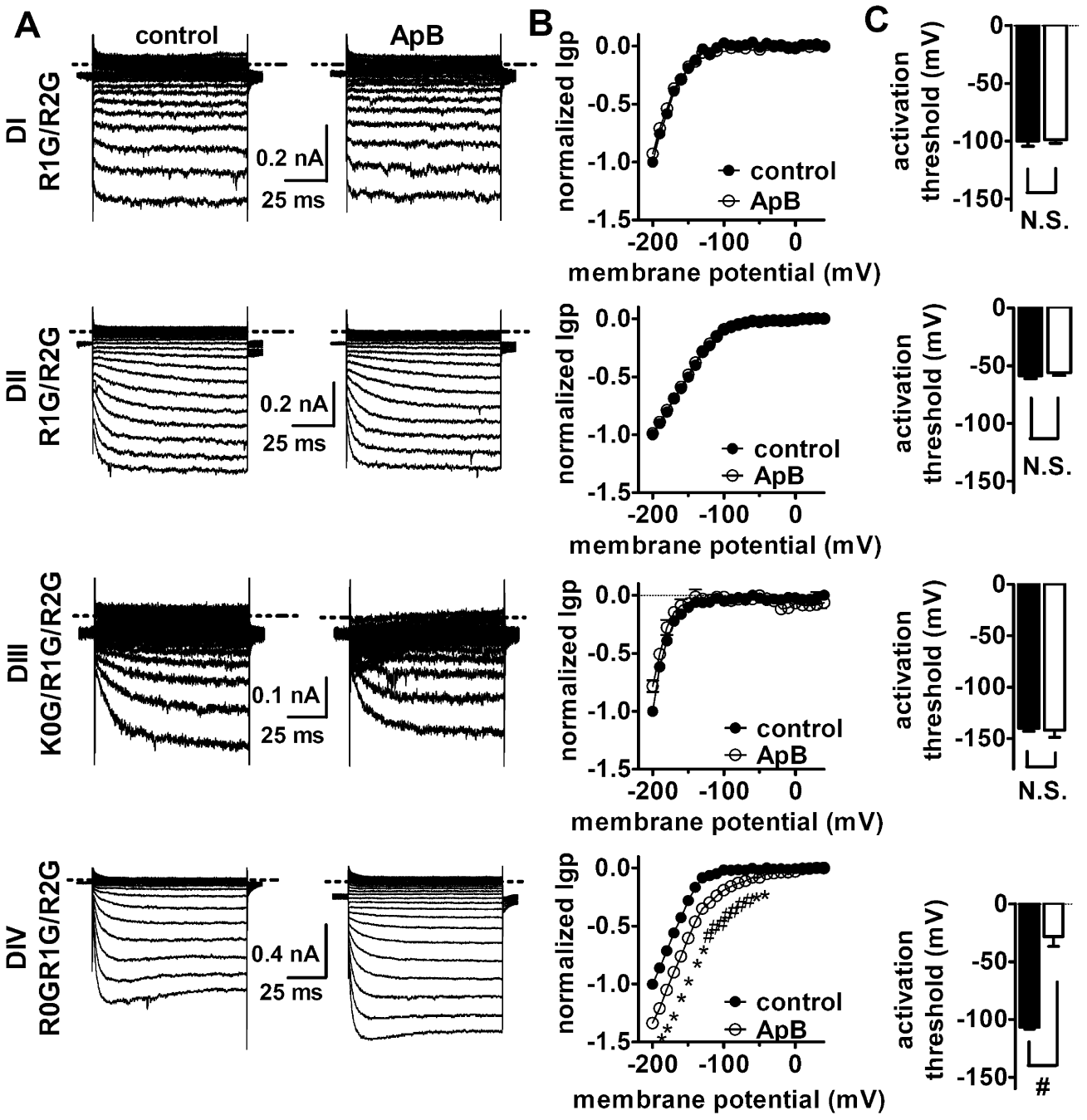
A
control
ApB
DI
R1G/R2G
0.2 nA
25 ms
DII
R1G/R2G
0.2 nA
25 ms
DIII
K0G/R1G/R2G
0.1 nA
25 ms
DIV
R0GR1G/R2G
0.4 nA
25 ms
B
normalized Igp
0.0
-0.5
-1.0
-1.5
-200
-100
0
membrane potential (mV)
control
ApB
C
activation threshold (mV)
0
-50
-100
-150
N.S.
N.S.
N.S.
#

Figure 6

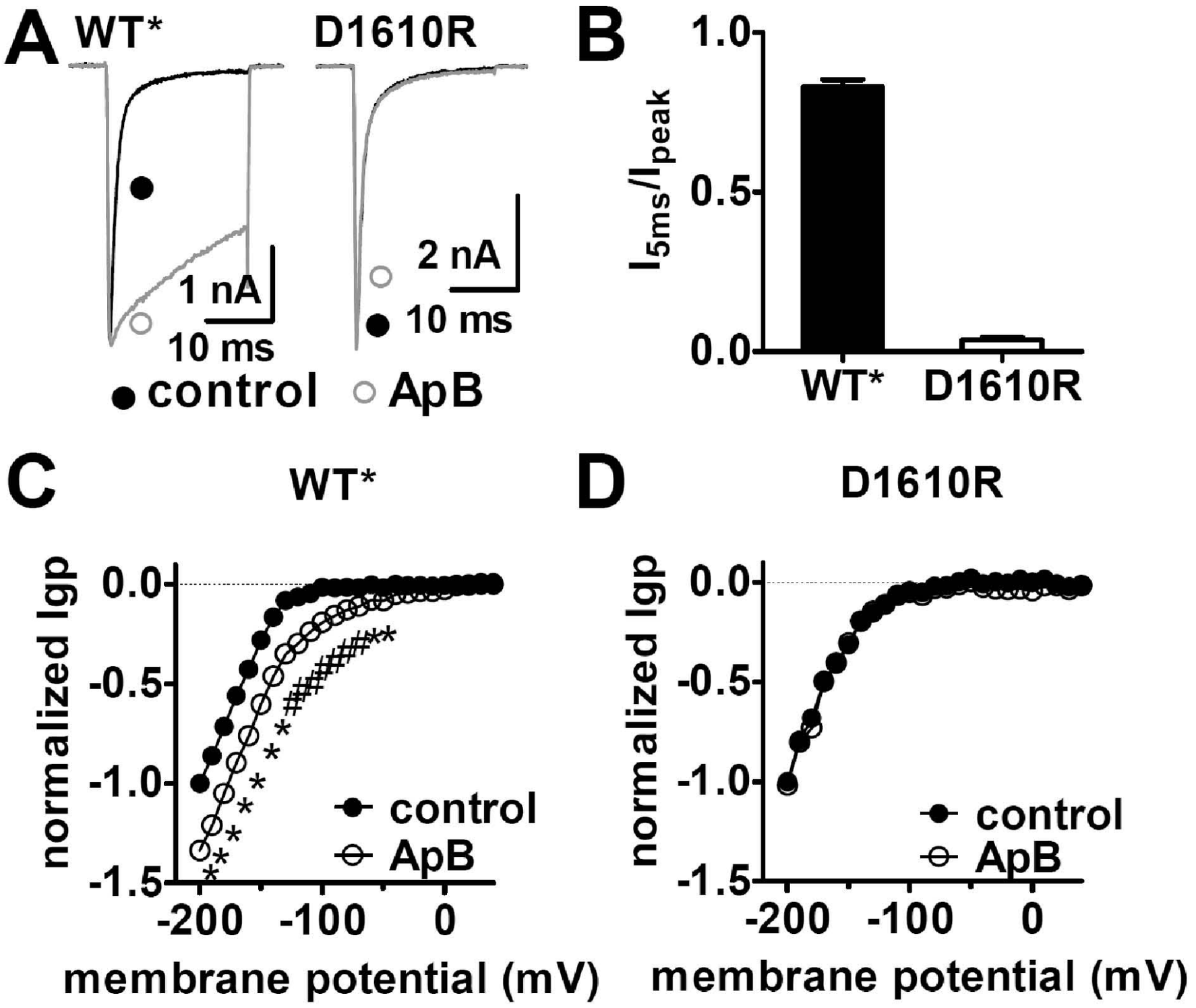
A
WT*
D1610R
1 nA
10 ms
2 nA
10 ms
control
ApB
B
1.0
0.5
0.0
I_{5ms}/I_{peak}
WT*
D1610R
C
WT*
normalized Igp
0.0
-0.5
-1.0
-1.5
-200
-100
0
control
ApB
membrane potential (mV)
D
D1610R
normalized Igp
0.0
-0.5
-1.0
-1.5
-200
-100
0
control
ApB
membrane potential (mV)

Figure 7

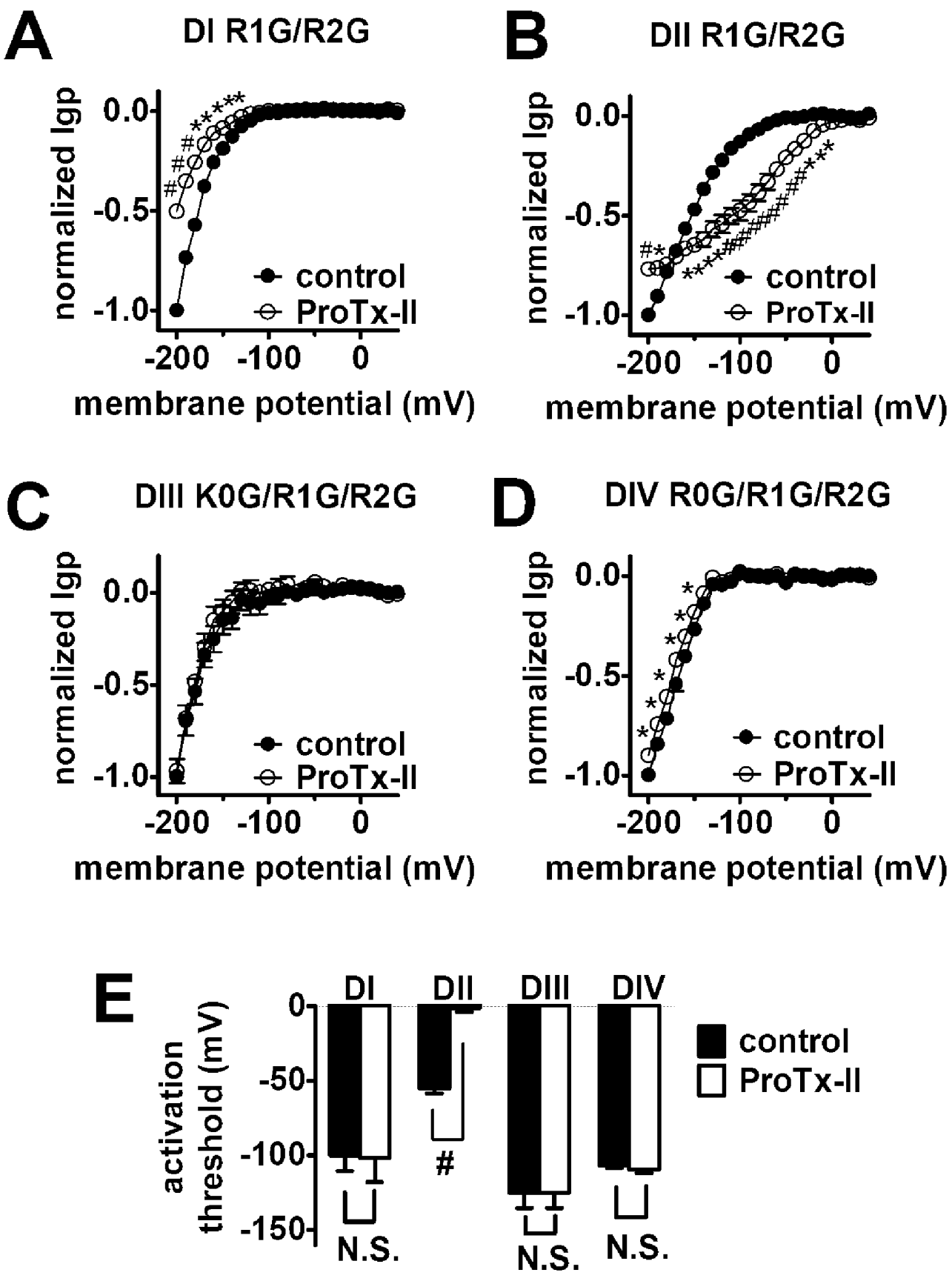
A
DI R1G/R2G
normalized Igp
0.0
-0.5
-1.0
-200
-100
0
membrane potential (mV)
control
ProTx-II
B
DII R1G/R2G
normalized Igp
0.0
-0.5
-1.0
-200
-100
0
membrane potential (mV)
control
ProTx-II
C
DIII K0G/R1G/R2G
normalized Igp
0.0
-0.5
-1.0
-200
-100
0
membrane potential (mV)
control
ProTx-II
D
DIV R0G/R1G/R2G
normalized Igp
0.0
-0.5
-1.0
-200
-100
0
membrane potential (mV)
control
ProTx-II
E
activation threshold (mV)
0
-50
-100
-150
DI
DII
DIII
DIV
N.S.
#
N.S.
N.S.
control
ProTx-II

Figure 8

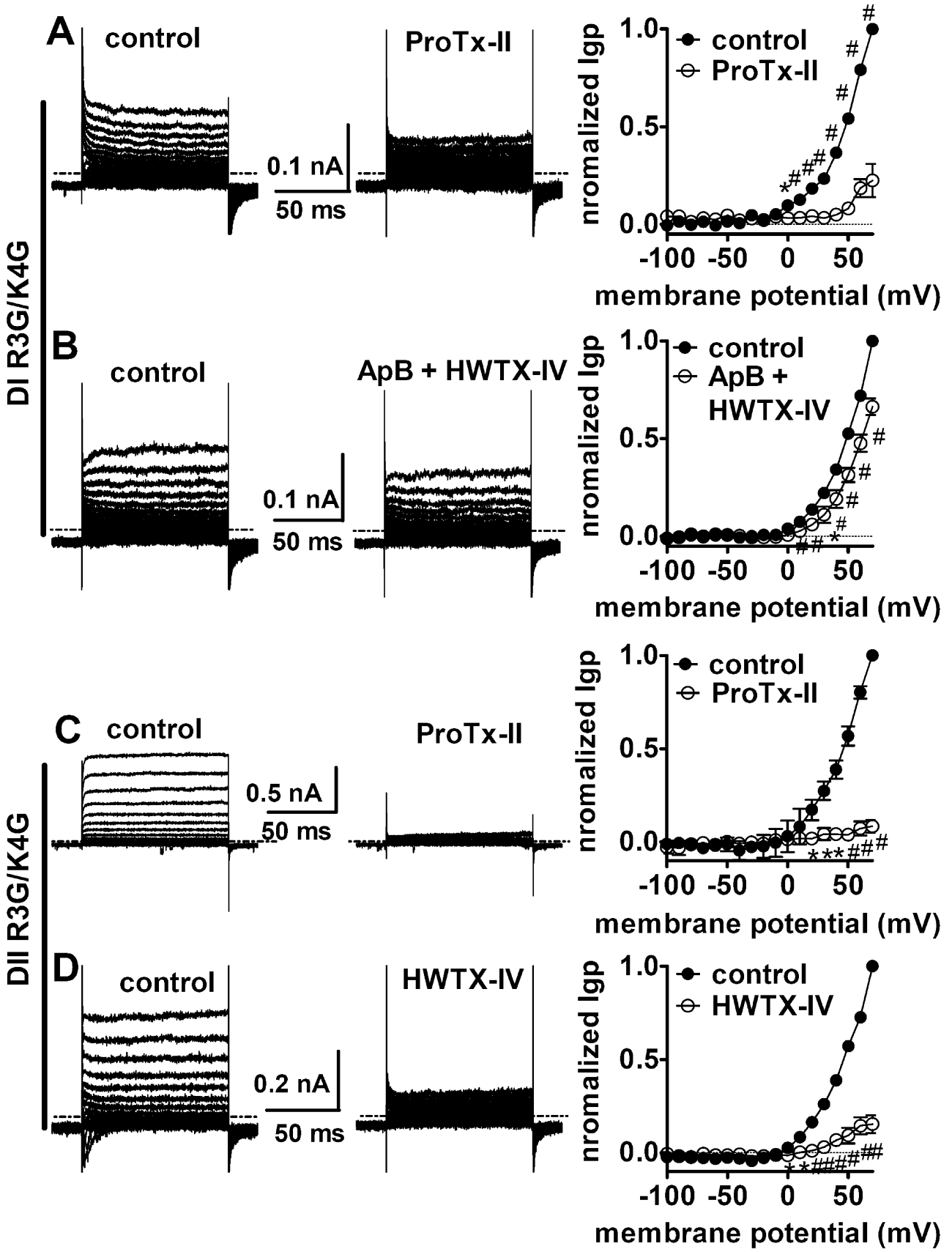
A
control
ProTx-II
0.1 nA
50 ms
DI R3G/K4G
B
control
ApB + HWTX-IV
0.1 nA
50 ms
C
control
ProTx-II
0.5 nA
50 ms
DII R3G/K4G
D
control
HWTX-IV
0.2 nA
50 ms
nromalized Igp
1.0
0.5
0.0
-100 -50 0 50
membrane potential (mV)
control
ProTx-II
ApB +
HWTX-IV
HWTX-IV